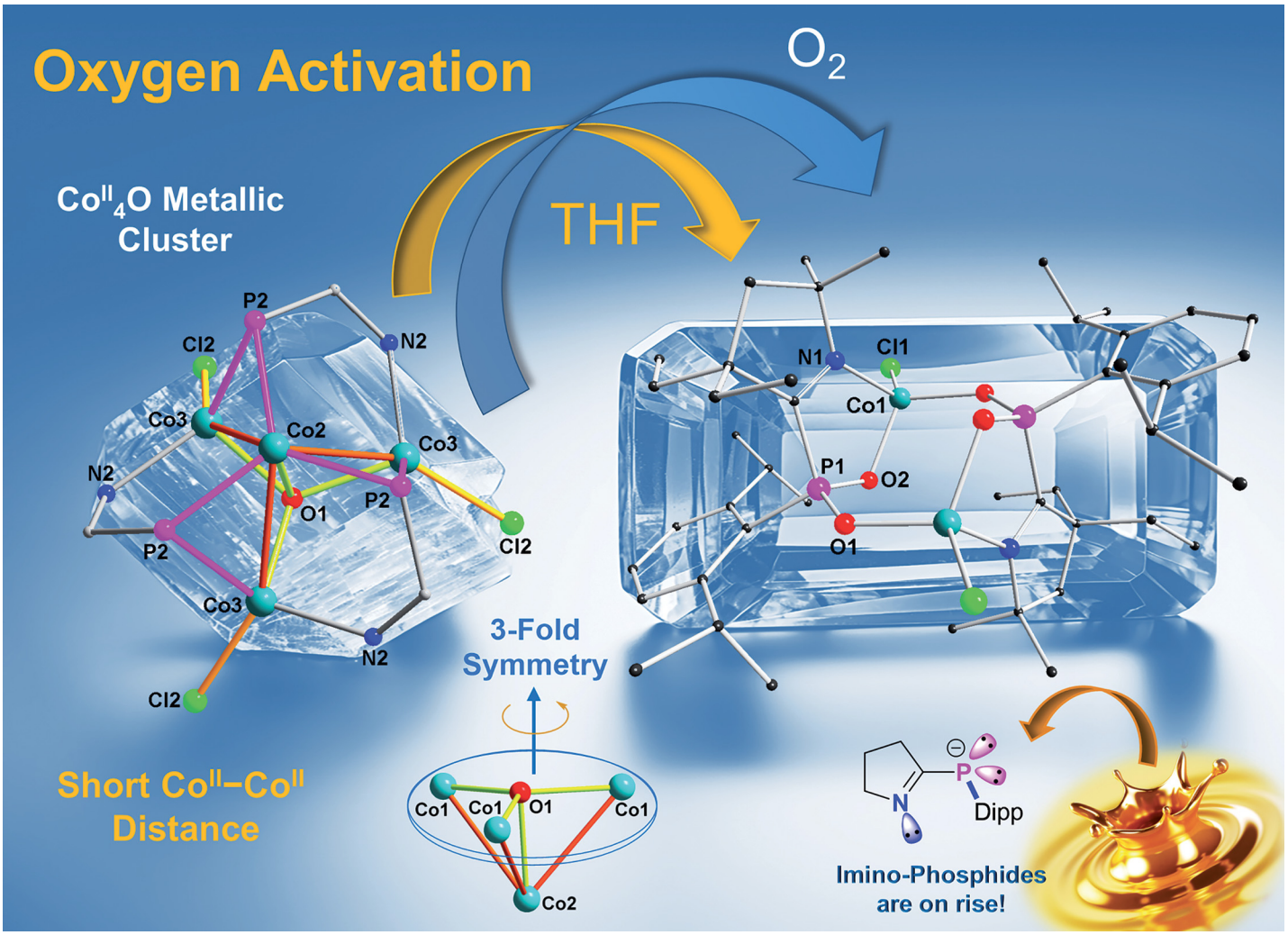

Showcasing research from Professor Roy's laboratory, Department of Chemistry, Indian Institute of Science Education and Research (IISER) Tirupati, Andhra Pradesh, India

Isolation and oxygen activation of electron-rich Co^{II}_4O metallic clusters having a 3-fold symmetry

Imino-phosphide ligands have been introduced for stabilization of atomically precise tetra-nuclear cobalt clusters with Co^{II}_4O core, and short Co–Co distances. The reactivity of these novel clusters has been explored towards activation of molecular di-oxygen, affording royal blue di-nuclear Co^{II} complexes.

Image reproduced by permission of Sudipta Roy from *Chem. Commun.*, 2025, **61**, 6897.

As featured in:

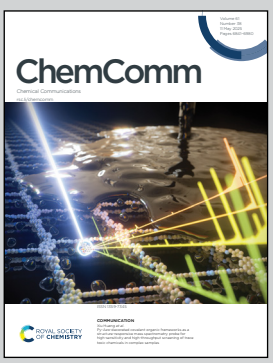

See Björn Schwarz, Sudipta Roy *et al.*, *Chem. Commun.*, 2025, **61**, 6897.

ROYAL SOCIETY OF CHEMISTRY

rsc.li/chemcomm

Registered charity number: 207890

ChemComm

COMMUNICATION

View Article Online
View Journal | View Issue

Cite this: *Chem. Commun.*, 2025, **61**, 6897

Received 13th December 2024,
Accepted 1st April 2025

DOI: 10.1039/d4cc06550f

rsc.li/chemcomm

Isolation and oxygen activation of electron-rich Co^{II}_4O metallic clusters having a 3-fold symmetry†

Maria Francis, [a] Asutosh Patra, [a] Farsana Abdul Salam, [a] Liviu Ungur, [b] Björn Schwarz *[c] and Sudipta Roy *[a]

Two novel atomically precise tetra-nuclear cobalt clusters (3a–3b) having a Co^{II}_4O core with 3-fold symmetry, and three short Co–Co distances of 2.7046(4) Å are isolated with three chelating NP-donor mono-anionic ligands. 3a–3b are shown to react with O_2, producing dinuclear cobalt complexes (4a–4b), where the P-centres of the ligands are oxygenated. All complexes are structurally characterized by single-crystal X-ray diffraction, and further studied by UV-vis, IR spectroscopy, CV, magnetic susceptibility measurements, and DFT calculations.

Metallic cobalt-clusters [Co_n/Co_nO] are known to exhibit numerous applications. Cobalt-carbonyls and their polynuclear analogues (Co_4, Co_{10}, *etc.*) have attracted chemists for their structural aspects, bonding, and unusually higher stability.[1] $Co_2(CO)_8$ is known for hydroformylation of olefins.[1] The stability, and bonding of metallic Co_n clusters (n = 4, 13) on the graphene surface have been studied by DFT calculation.[2] The Co_{13} cluster is known to absorb CO gas.[2d] The Co_4 coordination cluster is found to be effective in boosting the oxygen reduction of Fe–N–C catalysts with single-atom Fe–N_4 configurations.[3] Adsorption of H_2 on cobalt clusters Co_6 and Co_{13} has been studied by DFT calculations.[4] A hydrocarbon-soluble Co^{I}_4 nano-catalyst having the spin crossover property[5] is known to display excellent catalytic hydrogenation of unsaturated hydrocarbons at low temperature/pressure,[6] while the corresponding cation exhibited slow relaxation of magnetization having S = 9/2 spin ground state.[5] A Co_4 cluster on a graphdiyne surface acts as a catalyst for electro-chemical N_2 reduction producing ammonia.[7] Co_n[2a–c,8a,b] (n = 4, 6, 13), and Co_nO[8c] clusters (n = 2, 3, 11) have been deposited on surfaces, followed by utilization in hydrogenation, and oxygenation reactions.[8] Decomposition of N_2O/NO on Co_n clusters has been theoretically investigated.[9] Co-clusters confined in mesoporous silica nanospheres containing N-doped carbon have been shown to efficiently dissociate the O–O bond of peroxymonosulphate, producing $HO^{\bullet}$, and $SO_4^{\bullet-}$ radicals.[10] The sub-nanocluster Co_4-catalysts deposited on silanol nests containing both ionic Co–O, and metallic Co–Co bonds are known for efficient dehydrogenation of propane.[11]

Herein, we report on the solid-state isolation of highly air, and moisture-sensitive structurally well-defined organic solvent-soluble tetranuclear Co^{II}_4O metal-clusters **3a–3b**, and the corresponding oxygen-activated dimeric Co^{II}_2 complexes **4a–4b**.

A 1 : 2 molar mixture of the orange crystals of Cs-(Dipp)-cyclic alkyl(imino) phosphide (**1a**),[12] and anhydrous $CoCl_2$ was stirred in THF at rt for 12 h under an argon atmosphere. Upon filtration, the insoluble black precipitate was separated, and the concentrated dark bluish-black filtrate was stored at −40 °C in a freezer. After 3–4 weeks, dark bluish-black hexagonal crystals of [((Dipp)(Et_2-cAI)P(CoCl))$_3$(Co)O] (**3a**) were obtained in 35% yield (Scheme 1).

Colorless, manually separable needles of bis-(Dipp)(imino)-phosphene (**2a**) were produced after 2–3 days as the by-product in 29% isolated yield. When a similar reaction mixture as stated above with 1 : 2 molar ratio of **1a** and anhydrous $CoCl_2$, following 12 h of stirring at rt, was exposed to air for 15 min, bright blue blocks of the oxygen activated dimeric Co^{II}_2 complex [((Dipp)(Et_2-cAI)PO_2)$_2$($Co^{II}Cl_2$)] (**4a**) were isolated in 30% yield after 2–3 days of storing the concentrated reaction mixture at −40 °C in a freezer (Scheme 1). A 1 : 2 molar ratio of **1b**, and anhydrous $CoCl_2$ in THF at rt afforded highly crystalline tetranuclear Co^{II}_4 metal cluster [((Dipp)(Cy-cAI)P(CoCl))$_3$(Co)O] (**3b**) in 39% isolated yield (Scheme 1). Several attempts failed to produce good quality single crystals of **3b**, suitable for X-ray diffraction. Exposure of the above-mentioned reaction mixture to air afforded air-stable royal blue blocks of the Co^{II}_2 complex [((Dipp)(Cy-cAI)PO_2)$_2$-($Co^{II}Cl_2$)] (**4b**) from a freezer at −40 °C in 30% yield. The purity of the isolated crystals of **3a–3b**, and **4a–4b** has been confirmed by elemental analyses (see ESI†).

[a] *Department of Chemistry, Indian Institute of Science Education and Research (IISER) Tirupati, Tirupati – 517619, India. E-mail: roy.sudipta@iisertiruapti.ac.in*
[b] *Department of Chemistry, National University of Singapore, Singapore, Singapore*
[c] *Institute for Applied Materials (IAM), Karlsruhe Institute of Technology (KIT), Hermann-von-Helmholtz-Platz 1, Karlsruhe, D-76344, Germany. E-mail: bjoern.schwarz@kit.edu*

† Electronic supplementary information (ESI) available. CCDC: 2324725 (**2a**), 2324727 (**3a**), 2324726 (**4a**), 2344451 (**2b**), 2344452 (**4b**). For ESI and crystallographic data in CIF or other electronic format see DOI: https://doi.org/10.1039/d4cc06550f

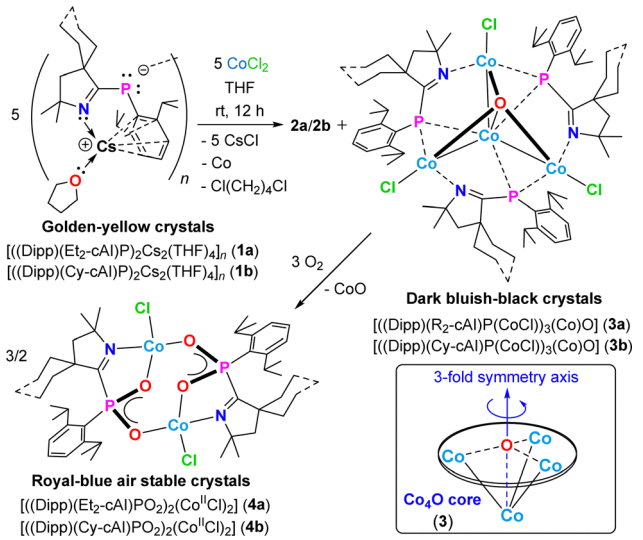

Scheme 1 Syntheses of Co^{II}_4O clusters **3a–3b** [Co1–Co2 2.7046(4)], and their reactivity with O_2 affording dimeric Co^{II}_2 complexes **4a–4b**. **2a–2b** are the respective bis-(Dipp)(imino)-phosphene by-products, isolated separately as white needles (see ESI†).

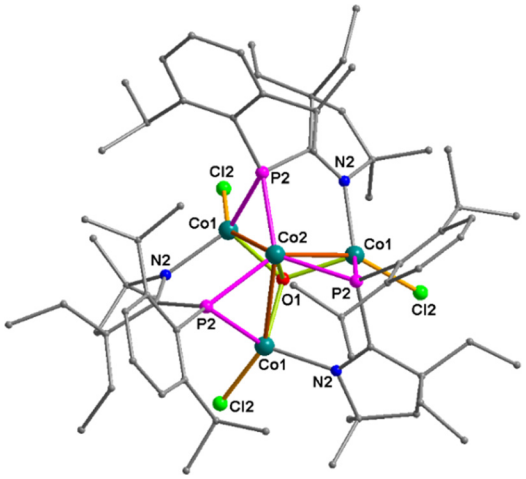

Fig. 1 Molecular structure of the Co^{II}_4 metal cluster [((Dipp)(Et2-cAl)P(CoCl))3(Co)O] (**3a**). Hydrogen atoms are omitted for clarity. Important bond lengths [Å], and bond angles [°]: Co1–Co2 2.7046(4), Co1–O1 1.9589(3), Co1–Cl1 2.2395(5), Co2–O1 2.036(2), Co2–P1 2.2808(4), P1–C10 1.8397(17); C10–P1–Co2 113.94(6), C10–N1–Co1 127.76(12). A three-fold axis is present along the Co2–O1 bond.

The Co^{II}_4 clusters **3a–3b** were highly air and moisture-sensitive. **3a–3b** were highly soluble in polar solvents, such as THF and DCM. The crystalline solids, and THF and/or DCM solutions of **3a–3b** were stable at rt under an argon atmosphere for more than 6 months. The powders of **3a–3b** were melted to yellow liquids at 209–210, and 211–212 °C, respectively. The dimeric Co^{II}_2 complexes **4a–4b** were air stable for a week, and sparingly soluble in THF. The powders of **4a–4b** were melted to yellow liquids under an argon atmosphere at 175–177, and 174–176 °C, respectively.

3a–3b have been characterized by IR, and UV-vis spectroscopy (see ESI†). The UV-vis absorption spectrum of the DCM solution of **3a** showed broad absorption bands with the corresponding maxima at 596 nm, and 597 nm with molar absorption coefficient (ε) values of 4862.38 and 229.35 M^{-1} cm^{-1}, respectively. Whereas, **4a** exhibited the absorption maxima at 289, 589, and 657 nm with ε values of 3283.01, 113.20, and 273.58 M^{-1} cm^{-1}, respectively (see ESI†). The computed IR_{P-O} stretching frequencies for the PO_2^- moiety in the model complex **4b′** were found to be 1067.16 cm^{-1}, and 1213.93 cm^{-1} for the symmetric and asymmetric modes, respectively, which were comparable with the experimental IR_{P-O} stretching frequencies observed for **4a–4b** (1070, 1210 cm^{-1} for **4a**; 1084, 1259 cm^{-1} for **4b**). These frequencies can be well compared with the reported stretching frequencies observed in L:$(O)_2$P–P$(O)_2$:L (L:=:C{N(2,6-$Pr^i_2C_6H_3$)CH}$_2$) (1279 cm^{-1}, 1061 cm^{-1}),[13] [(PO_2){Re(PyrPz)(PNP)}] (1263 cm^{-1}, 1086 cm^{-1}),[14] and the reported data for the free PO_2^- anion in a KCl matrix (1097 cm^{-1}, 1207 cm^{-1}).[15]

3a and **4a–4b** have been structurally characterized by single-crystal X-ray diffraction (Fig. 1 and 2, see ESI†). **3a** crystallizes in the trigonal *R*3*c* space group with a 3-fold rotational axis of symmetry passing through the Co2–O1 bond (2.036(2) Å) (Fig. 1). The structural feature of **3a** can be correlated with a stemless mushroom possessing three Co^{II} ions (three Co1 centres; Co–O distance of 1.9589(3) Å) in the periphery and a Co^{II} centre (Co2) at the top. All four Co^{II} atoms are connected through the μ_4-O atom, which lies 0.16 Å above the plane of the three peripheral Co^{II} ions (Co1), whereas the central Co2 atom is 1.87 Å below this plane. The Co2 atom is also 0.09 Å away from the plane containing three P1 atoms of the three (Dipp)-cyclic alkyl(imino) phosphide [(Dipp)(cAl)P^-] ligands. The Co1–Co2 distance in **3a** is found to be 2.7046(3) Å, which is significantly longer than that of the Co–Co distances present in the previously reported complexes $[(IMe_4)_2M(\mu\text{-PMes})]_2$ (M = Co) (2.5241(9) Å),[16] and triply μ-O_{alkoxy} bridged Co^{III}-complex $[[Co^{III}_2(hep)_3(N_3)_3]\cdot DMF]$ (2.595(6) Å),[17] but slightly longer than that of $(Me_2$-cAAC:$)_2Co_2$ (2.6550(6) Å).[18] The Co1–P1, and Co2–P1 bond distances in **3a** are found to be 2.4171(5) Å, and

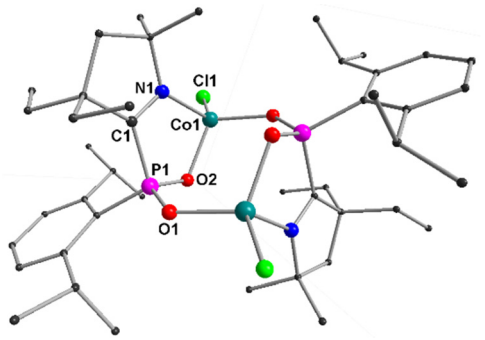

Fig. 2 Molecular structure of [((Dipp)(Et2-cAl)$PO_2)_2$($Co^{II}Cl)_2$] (**4a**). Hydrogen atoms are omitted for clarity. Co2 and O1 have 0.33 occupancy each. The ethyl group (C9 C10) is disordered with a site occupancy ratio of 53 : 47. Important bond lengths [Å], and bond angles [°]: Co1–Cl1 2.2034(11) [2.204], Co1–O1 1.941(2) [1.933], Co1–N1 2.042(3) [1.912], P1–O2 1.512(3) [1.554], P1–O1 1.514(3) [1.539], P1–C1 1.843(4) [1.824], N1–C1 1.282(5) [1.296]; O2–P1–O1 113.39(15) [114.96], P1–O2–Co1 115.66(15) [116.31].

2.2808(4) Å, respectively, in which the former one is comparable with that of the previously reported [Co{PH(IDipp)}{N(SiMe$_3$)$_2$}$_2$] complex (2.4572(8) Å).[19]

The P1–C10 bond distance in **3a** is found to be 1.8397(17) Å, which is typical of a P–C single bond. The N1–C10 bond length in complex **3a** is found to be 1.296(2) Å, which is comparable to that of complex **1a** (1.301(3) Å).[12]

The molecular structure of **4a** has been depicted in Fig. 2 (see ESI† for **4b**). **4a** crystallized in the monoclinic space group $P2_1/n$. The asymmetric unit of **4a** is composed of the monomeric unit [((Dipp)(cAl)PO$_2$)Co^{II}Cl]. The two Co^{II} ions in **4a** are bridged by the two $\mu_{1,3}$-Dipp-PO$_2^-$ moieties of the two PO$_2^-$ ligands through two O atoms of the PO$_2$ unit [*syn–anti*-bridging mode; PO$_2$Co$^{II}_2$] displaying the η^1:η^1:η^1:μ_2 bridging mode by the PO$_2$N donor set of the ligand. Each Co^{II} ion of **4a** is coordinated by one N atom of the [(Dipp)(cAl)P$^-$] ligand, while two O atoms of this ligand act as a *cis*-, *anti*-bridge between two Co^{II} ions. Finally, one terminal Cl atom completes the distorted tetrahedral geometry of each Co^{II} centre. The bond distances between Co1–O1/O2 are 1.941(2) Å, and 1.993(3) Å, respectively, where the former one is much shorter than the Co$_{peripheral}$–O distance (1.9589(3) Å), whereas, the latter one is comparable with the Co$_{apex}$–O distance (2.036(2) Å) observed in **3a**. The P–C bond distances [(1.843(4) Å] in **4a** correspond to the typical P–C single bond [P–C bond distance in NHC: → PCl$_3$ adduct is reported as 1.871(11) Å)], and are comparable to that of **3a** (1.8397(17) Å),[20] and slightly shorter than that of **2a** (1.8550(12) Å). The two P–O bond distances in **4a** are found to be almost identical (1.512(3) Å, 1.514(3) Å) representing the delocalization, which is also visible from the molecular orbitals in α-SOMO−58 and β-SOMO−52 (see ESI†). These bond lengths are slightly longer than the P–O distances found in NHC$_2$(PO$_2$)$_2$ (1.470(2)), (1.466(3) Å).[20] The distances between the two Co ions in **4a** and **4b** are found to be 4.247 and 4.40 Å, respectively, which are significantly longer than that in **3a** (2.7046(4) Å).

The electron paramagnetic resonance (EPR) spectrum of **3a** in DCM at 77 K exhibited a broad signal presumably due to the distorted tetrahedral geometry of Co1 (side), and Co2 (central) ions. The broadening of the EPR signal can be rationalized by the positive D values (−14.4, +32.4 cm^{-1}), and the rhombic nature of the Co(II) ions (see ESI†). The Mulliken spin density calculations (computed at UB3LYP-D3(BJ)/def2-TZVP level of theory) showed that the majority of the α-spin density of the model complex **3a′** (replacing Dipp groups by Me groups) is delocalized across the Co atoms (31.0%) located in the periphery, along with contributions from the central O atom (2.0%) and Cl atoms (1.2%) (Fig. 3).

In contrast, the β-spin density is primarily distributed over the Co (axial) and P atoms, with the largest contribution coming from the Co atom (95.0%).

The temperature-dependent magnetic susceptibility measurements performed on **3a** within the temperature range of 2–300 K revealed that the experimentally observed χT susceptibility *vs.* temperature values are slightly above the calculated molar Curie constant $C_{4Co(II)}$ = 7.50 cm^3 K mol^{-1} (dashed line in Fig. 4(a)) for four free high spin Co^{II} ions, each with spin S = 3/2

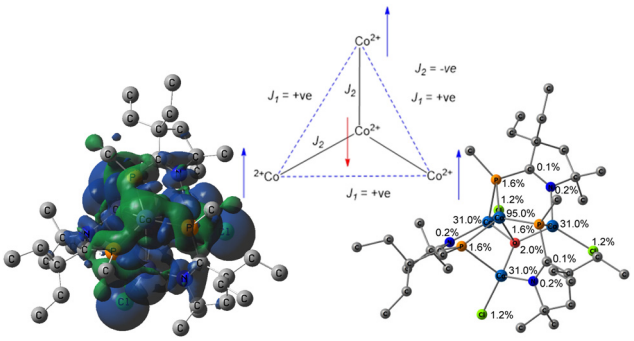

Fig. 3 Mulliken α-(blue), β-spin (green) densities of the model complex [((Me)(Et$_2$-cAl)P(CoCl))$_3$O] (**3a′**) at S = 3 (computed at the UB3LYP-D3(BJ)/def2-TZVP level of theory).

within a formula unit (f.u.), and without any interactions between each other. The slightly increased value is ascribed to weak dominant ferromagnetic (FM) interaction as already indicated by the positive Weiss constant obtained from the Curie–Weiss fit (see ESI†).

For the magnetic model, a total spin S = 3/2 was ascribed to each Co site. The three Co1 (side) are exchange coupled *via* the isotropic exchange constant J_1 with each other, and each Co1 is coupled *via* J_2 to the central Co2 ion. Utilizing the program PHI,[21] isotropic exchange parameters were refined to J_1 = 18.52(5) cm^{-1}, and J_2 = −15.15(5) cm^{-1}, *i.e.* with a slightly dominant FM exchange interaction as also found by Curie–Weiss fit. Furthermore, the ZFS parameters (only the axial D parameter has been used for the applied model here) were refined to D(Co1) = −14.4(1) cm^{-1}, and D(Co2) = 32.4(1) cm^{-1}. The antiferromagnetic coupling between Co1 (side) and Co2 (central) creates a ground state with reduced magnetic moment due to the mutual partial cancelling out, and furthermore, the ZFS reduces the measured magnetization, especially at low temperature due to the single-ion anisotropy that forces the magnetic moments to be aligned along the statistically distributed (polycrystalline sample) uniaxial anisotropy axes (D).[22] The spin ground state of the previously reported (NHC)$_4$Co$^{II}_4$S$_4$ cluster with Co–Co distances of ∼2.69 Å was found to be S = 3 (see ESI†).[23]

The natural bond orbital (NBO) analysis performed on model complex **3a′** (calculated at UB3LYP/def2-TZVP level of theory) in

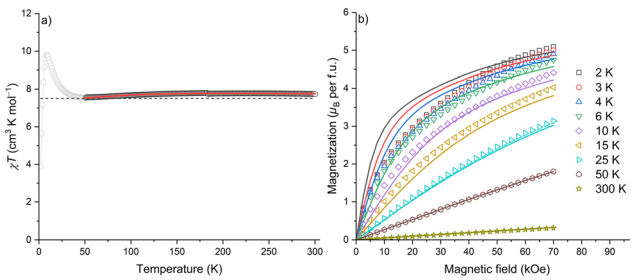

Fig. 4 Experimental (open symbols), and simulated (solid lines) (a) χT *vs.* T, and (b) magnetization *vs.* magnetic field plots for **3a**. The dashed line in (a) represents the calculated molar Curie constant, $C_{4Co(II)}$ = 7.50 cm^3 K mol^{-1} for four free Co^{II} ions, each with spin S = 3/2 per f.u.

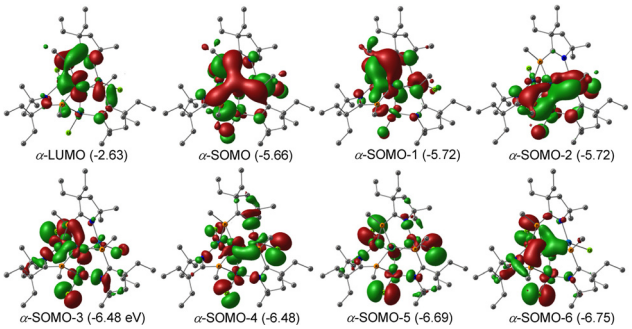

Fig. 5 Selected Kohn–Sham orbitals of the model complex [((Me)(Et_2-cAl)P(CoCl))$_3$O] (**3a′**) at the *S* = 3 (at UB3LYP-D3(BJ)/def2-TZVP level of theory; energies given in parentheses are in eV).

the septet state revealed that the α-SOMO corresponds to the delocalization of electrons on Co and O on the axial position, and P atoms on the periphery (Fig. 5). The α-SOMO−1 corresponds to the 3-centered electron delocalization over the $Co_{periphery}$–P–Co_{axial} moiety, where the major coefficient resides on the p-orbital of P (75.6%). The α-SOMO−5 corresponds to the σ-electron donation from O atom (83.5%) to the Co present at the axial position.

The EPR spectrum of **4a–4b** in DCM at 298 K exhibited the signal with a g_{eff} value of 2.0053 and 2.0829, respectively (see ESI†). The α-spin density of **4b** is predominantly found on the Co ions (45.6%), where the unpaired electron exists with only minimal contributions from O (0.69%, 0.62%), P (0.3%), and the ligand (C 0.1%; N 0.6%) (see ESI†).

The DC magnetic susceptibility measurements of **4b** showed that the magnetic momentum per Co-ion is significantly higher than that of **3a** (see ESI†). The χT product is 7.65 cm^3 K mol^{-1} at 300 K, which slowly decreases to 6.77 cm^3 K mol^{-1} at 28 K due to the spin–orbit-coupling of Co^{II} ions (see ESI†).

In conclusion, we have developed a novel strategy for solid state isolation of the highly moisture, and oxygen-sensitive structurally well-defined Co_4^{II} metal clusters, **3a–3b** with the Co_4O core by reacting the Cs-salts **1a–1b** with anhydrous $CoCl_2$ at rt under an argon atmosphere. The Mulliken spin density calculations on **3a′** revealed delocalized α-spin density across the peripheral Co ions with smaller contributions from central O and Cl atoms. **3a–3b** were successfully utilized for the activation of aerial O_2 affording air-stable dimeric Co^{II} complexes **4a–4b.**

SR gratefully acknowledges STARS-IISC-MoE, (MoE-STARS/STARS-2/2023-0666), and IISER Tirupati for financial support. We acknowledge Subuhan Ahamed (IIT Madras) for generating the Hirshfeld plots, and EPR simulation.

Data availability

The data supporting this article (syntheses, UV-Vis, EPR, XPS, single-crystal X-ray data, magnetic data, and computational details) are included as part of the ESI.† Crystallographic data for **2a–2b**, **3a**, and **4a–4b** have been deposited at the CCDC (2324725–2324727, 2344451 and 2344452†), which can be obtained from **https://www.ccdc.cam.ac.uk/**.

Conflicts of interest

There are no conflicts to declare.

Notes and references

1 (*a*) L. P. Battaglia, D. Delledonne, M. Nardelli, G. Predieri, G. P. Chiusoli, M. Costa and C. Pelizzi, *J. Organomet. Chem.*, 1898, **363**, 209; (*b*) C. Xia, K. Yang, S. G. Bott and M. G. Richmond, *Organometallics*, 1996, **15**, 4480; (*c*) M. Costa, G. Gervasio, D. Marabello and E. Sappa, *J. Organomet. Chem.*, 2002, **656**, 57; (*d*) F. Mafuné, Y. Wu, M. Yamaguchi and S. Kudoh, *J. Phys. Chem. A*, 2024, **128**, 3516.
2 (*a*) L. Liu, Y. Su, J. Gao and J. Zhao, *Physica E*, 2012, **46**, 11; (*b*) T. Alonso-Lanza, A. Ayuela and F. Aguilera-Granja, *ChemPhysChem*, 2015, **16**, 3700; (*c*) K. García-Díez, J. Fernández-Fernández, J. A. Alonso and M. J. López, *Phys. Chem. Chem. Phys.*, 2018, **20**, 21163; (*d*) Y. Wang, L. Wang and S. Ma, *Appl. Surf. Sci.*, 2019, **481**, 1080.
3 A. Han, W. Sun, X. Wan, D. Cai, X. Wang, F. Li, J. Shui and D. Wang, *Angew. Chem., Int. Ed.*, 2023, **62**, e202303185.
4 K. García-Díez, J. Fernández-Fernández, J. A. Alonso and M. J. López, *Phys. Chem. Chem. Phys.*, 2018, **20**, 21163.
5 K. Chakarawet, P. C. Bunting and J. R. Long, *J. Am. Chem. Soc.*, 2018, **140**, 2058.
6 J. Camacho-Bunquin, M. J. Ferguson and J. M. Stryker, *J. Am. Chem. Soc.*, 2013, **135**, 5537.
7 Y. Luo, M. Li, Y. Dai, R. Zhao, F. Jiang, S. Wang and Y. Huang, *Inorg. Chem.*, 2021, **60**, 18251.
8 (*a*) J. L. Rodríguez-López, F. Aguilera-Granja, K. Michaelian and A. Vega, *Phys. Rev. B: Condens. Matter Mater. Phys.*, 2003, **67**, 174413; (*b*) F. Mafuné, Y. Wu, M. Yamaguchi and S. Kudoh, *J. Phys. Chem. A*, 2024, **128**, 3516; (*c*) S. Lee, A. Halder, G. A. Ferguson, S. Seifert, R. E. Winans, D. Teschner, R. Schlögl, V. Papaefthimiou, J. Greeley, L. A. Curtiss and S. Vajda, *Nat. Commun.*, 2019, **10**, 954.
9 J. Facio-Muñoz, D. Hernández-Velázquez, G. Guzmán-Ramírez, R. Flores-Moreno, J. Rodriguez-Zavala and F. Tenorio, *J. Mol. Model.*, 2022, **28**, 197.
10 X. Xie, M. Zhu, F. Xiao, Y. Xiang, H. Zhong, Z. Ao and H. Huang, *JACS Au*, 2023, **3**, 1496.
11 W. Deng, D. He, D. Chen, Z. Huang, J. Deng and Y. Luo, *Commun. Mater.*, 2024, **5**, 215.
12 E. Nag, M. Francis, D. Putta and S. Roy, *Chem. – Eur. J.*, 2023, e202302120.
13 Y. Wang, Y. Xie, P. Wie, H. F. Schaefer III, P. V. R. Schleyer and G. H. Robinson, *J. Am. Chem. Soc.*, 2013, **135**, 19139.
14 J. Abbenseth, F. Wätjen, M. Finger and S. Schneider, *Angew. Chem., Int. Ed.*, 2020, **59**, 23574.
15 S. J. Hunter, K. W. Hipps and A. H. Francis, *Chem. Phys.*, 1979, **39**, 209.
16 K. Pal, O. B. Hemming, B. M. Day, T. Pugh, D. J. Evans and R. A. Layfield, *Angew. Chem., Int. Ed.*, 2016, **55**, 1690.
17 J. Kumar, N. S. M. Gorantla, S. Roy, A. N. Paesch, R. Herbst-Irmer, D. Stalke, C. Anusha, S. De, P. Parameswaran, H. W. Roesky and K. C. Mondal, *ChemistrySelect*, 2018, **3**, 8221.
18 K. C. Mondal, P. P. Samuel, H. W. Roesky, E. Carl, R. HerbstIrmer, D. Stalke, B. Schwederski, W. Kaim, L. Ungur, L. F. Chibotaru, M. Hermann and G. Frenking, *J. Am. Chem. Soc.*, 2014, **136**, 1770.
19 R. Weller, A. Gonzalez, H. Gottschling, C. von Hänisch and W. C. Gunnar, *Z. Anorg. Allg. Chem.*, 2022, **648**, e202100338.
20 Y. Wang, Y. Xie, M. Y. Abraham, R. J. Jr, P. Wei, H. F. III Paul and G. H. Robinson, *Organometallics*, 2010, **29**, 4778.
21 N. F. Chilton, R. P. Anderson, L. D. Turner, A. Soncini and K. S. Murray, *J. Comput. Chem.*, 2013, **34**, 1164.
22 B. Schwarz and Q. Fu, *Eur. J. Inorg. Chem.*, 2024, e202400162.
23 L. Deng, E. Bill, K. Wieghardt and R. H. Holm, *J. Am. Chem. Soc.*, 2009, **131**, 11213.

